10. E. Hirsinger *et al.*, *Development* **128**, 107 (2001).

11. C. Shawber *et al.*, *Development* **122**, 3765 (1996).

12. K. Kuroda *et al.*, *J Biol Chem* **274**, 7238 (1999).

13. X. Gao *et al.*, *J Cell Biol* **154**, 1161 (2001).

14. J. Cossins, A. E. Vernon, Y. Zhang, A. Philpott, P. H. Jones, *Development* **129**, 2195 (2002).

15. D. Selkoe, R. Kopan, *Annu Rev Neurosci* **26**, 565 (2003).

16. I. Delgado *et al.*, *Genomics* **82**, 109 (2003).

17. I. M. Conboy, T. A. Rando, *Dev Cell* **3**, 397 (2002).

J Neuropathol Exp Neurol

Vol. 64, No. 12
December 2005
pp. 1108–1117

ORIGINAL ARTICLE

Behavioral and Histological Evaluation of a Focal Cerebral Infarction Rat Model Transplanted With Neurons Induced from Bone Marrow Stromal Cells

Toshiro Mimura, MD, PhD, Mari Dezawa, MD, PhD, Hiroshi Kanno, MD, PhD, and Isao Yamamoto, MD, PhD

Abstract

Neurons can be specifically induced from bone marrow stromal cells (MSCs) with extremely high efficiency using gene transfection of the Notch intracellular domain and subsequent treatment with basic-fibroblast growth factor, forskolin, and ciliary neurotrophic factor. We investigated the behavioral and histologic efficacy of such bone marrow stromal cell-derived neuronal cell (MSDNC) transplantation into a focal cerebral infarction model in rats. A left middle cerebral artery occlusion (MCAO) was performed on adult Wistar rats. MSDNC transplantation into the ipsilateral hemisphere was performed on day 7 after MCAO. The behavioral analyses were conducted on days 14, 21, 28, 35, and 36–40, and a histologic evaluation was performed on day 41. MSDNC-transplanted rats showed significant recovery compared with controls (MCAO without cell transplantation) in beam balance, limb placing, and Morris water maze tests. Histologically, transplanted cells migrated from the injection site into the ischemic boundary area, including the cortex, corpus callosum, striatum, and hippocampus. Transplanted MSDNCs were positive for MAP-2 (84% ± 8.11%), whereas only a small number of cells were positive for GFAP (1.0% ± 0.23%). The survival rates of MSDNCs and MSCs 1 month after transplantation were approximately 45% and 10%, respectively. These results suggest that use of MSDNCs may be a promising therapeutic strategy for cerebral infarction.

Key Words: Behavioral analysis, Bone marrow stromal cell, Immunohistochemistry, Middle cerebral artery occlusion (MCAO), Transplantation.

From the Department of Neurosurgery (TM, HK, IY), Yokohama City University Graduate School of Medicine, 3–9 Fukuura, Kanazawa-ku, Yokohama, Japan; and the Department of Anatomy and Neurobiology (MD), Kyoto University Graduate School of Medicine, Yoshidakonoe-cho, Sakyo-ku, Kyoto, Japan.

Send correspondence and reprint requests to: Toshiro Mimura, MD, PhD, Department of Neurosurgery, Yokohama City University Graduate School of Medicine, 3-9 Fukuura, Kanazawa-ku, Yokohama, 236-0004 Kanagawa, Japan; E-mail: mimura-nsu@umin.ac.jp

This study was supported by a Grant-in-Aid (no.13557120, no.15590166, and no.15016091) from the Ministry of Education, Science and Culture of Japan.

INTRODUCTION

In the central nervous system, neural tissue that is irreversibly damaged by ischemic injury enters the process of necrosis. Although intrinsic progenitor cells proliferate and differentiation takes place, these progenitor cells are insufficient for full functional recovery (1).

Neural cell transplantation into the ischemic brain has been reported in animal models, and amelioration of somatosensory and cognitive function has often been shown in these models (2, 3). However, currently, donor cells such as neural stem cells (NSCs) can only be supplied from the fetus forebrain or the subventricular zone of the adult brain. Additional problems include an inadequate supply of NSCs on a therapeutic scale and ethical concerns regarding their use. Furthermore, there is a problem of contamination by glial cells during neural differentiation.

Bone marrow stromal cells (MSCs) can differentiate into other cell types such as osteoblasts, adipocytes, chondrocytes, and cardiomyocytes (4–8). MSCs are promising candidates for clinical application because they are easy to isolate from bone marrow aspirates and are readily expanded in vitro, and they can be used for autotransplantation without posing major ethical problems. Several reports have shown that MSCs can differentiate into neural lineages; for example, neuron-like cell induction from MSCs with some accompanying induction of glial cells has been demonstrated in vitro (9–11). However, the induction efficiency of neurons is low, and functional recovery after transplantation of induced neural cells in animal models of neuronal disorder has not been tested.

Dezawa et al recently reported that neuronal cells can be specifically induced with extremely high efficiency from MSCs by introduction of the Notch intracellular domain followed by administration of basic-fibroblast growth factor, ciliary neurotrophic factor, and forskolin without the occurrence of glial differentiation (12). The MSC-derived neuronal cells (MSDNCs) expressed neuronal markers immunohistochemically and showed neuronal properties in an electrophysiological analysis. Transplantation of these MSDNCs resulted in improvement in apomorphine-induced rotational behavior after intrastriatal implantation in a 6-hydroxydopamine rat model of Parkinson disease (12).

In this study, we induced MSDNCs from adult rat MSCs and transplanted the cells into the infarct area in a middle cerebral artery occlusion (MCAO) rat model. Behavioral tests

and histologic assessment were conducted after transplantation. Our results show that MSDNCs are effective in the amelioration of damage in an ischemic rat model.

MATERIALS AND METHODS

All experimental procedures were approved by the Animal Experimentation Ethics Committee of Yokohama City University School of Medicine.

Culturing of Marrow Stromal Cells and Neuronal Induction

MSCs were isolated from 8-week-old Wistar rats as described previously (13). The MSCs were labeled with green fluorescent protein (GFP) by retroviral infection using the pBabe neo-GFP vector (14).

Neuronal induction from MSCs has been described by Dezawa et al (12). Briefly, MSCs subcultured four times were transfected with a vector (pCI neo-NICD) containing the Notch1 intracellular domain (NICD) using Lipofectamine 2000 (Invitrogen Corp., Carlsbad, CA). Cells were selected by G418 treatment for 11 days. For induction of MSDNCs, NICD-transfected MSCs were subcultured once (60–70% confluence) and were incubated in alpha-MEM containing 10% FBS, 5 μM forskolin (Calbiochem, La Jolla, CA), 10 ng/mL basic-fibroblast growth factor (Peprotech, London, U.K.), and 10 ng/mL ciliary neurotrophic factor (R&D Systems, Minneapolis, MN). Five days later, cells were transplanted into the MCAO rat model. To characterize the induced MSDNCs in vitro, we performed immunocytochemistry. Anti-MAP-2ab (Sigma, St. Louis, MO), neurofilament-M (NF-M) (Chemicon, Temecula, CA) and beta-tubulin isotype-3 (β-tubulin-3) (Sigma) were used as neuronal markers.

Middle Cerebral Artery Occlusion Rat Model

Male Wistar rats weighing 200 to 250 g were kept at room temperature (24°C) with a 12-hour light–dark cycle and were given food and water freely. The MCAO procedure was a modification of the methods of Koizumi (15) and Longa (16). Briefly, under deep anesthesia induced by a mixture of 1.0% to 1.5% halothane, 10% O_2, and air, a midline cervical incision was performed and the left carotid bifurcation was identified. A probe made of 4-0 nylon thread with a silicon rubber-coated head of diameter 0.3 mm was inserted into the ligated external carotid artery and advanced into the internal carotid artery to a position 16 to 18 mm from the bifurcation. During the surgery, rectal temperature was maintained between 37.5°C and 38°C using a feedback heating pad (BWT-100; Bio Research Center Co. Ltd., Tokyo, Japan). Arterial blood gas analysis was performed and pO_2 was maintained at 85 to 120 mm Hg through control of the anesthetic device. Reperfusion was performed 4 hours after the occlusion through a 10-mm withdrawal of the probe.

Transplantation

On day 7 after MCAO, rats were anesthetized with intraperitoneal injection of 50 mg/kg sodium pentobarbital and placed onto a stereotaxic frame. In a preliminary experiment, the infarct area was produced in the lateral area from approximately 3.5 mm lateral to the midline. For transplantation into the nonnecrotic brain parenchyma, the cell suspension, composed of 8,000 to 16,000 cultured cells in 3 μL of phosphate-buffered saline (PBS, pH 7.4), was stereotaxically injected into the left forebrain from the following three locations: +2 mm, 0 mm, and −2 mm anterior to the bregma, and 2 mm lateral to the midline, and at 1.2 mm depth from the cortical surface in each case. The total number of transplanted cells was 24,000 to 48,000.

Three groups of animals were prepared: 1) the control group, which received only PBS (without cell transplantation) (n = 7); 2) the MSC group, which underwent transplantation of nontreated intact MSCs (n = 10); and 3) the N-MSC group, into which MSDNCs were transplanted (n = 10).

Behavioral Testing

The severity of neurologic damage was evaluated using the following tests: a beam balance test, a limb placing test, and a Morris water maze test. The beam balance test and the limb placing test were performed on days 7 (just before transplantation), 14, 21, 28, and 35 after MCAO. The Morris water maze test was performed from days 36 to 40.

Beam Balance Test

The beam balance test is used to assess gross vestibulomotor function and was carried out as described previously (17). Scoring was based on the following criteria: balancing with a steady posture with paws on the top of the beam: a score of zero; grasping the sides of the beam and/or shaky movement: one; one or more paw(s) slipping off the beam: 2; attempting to balance on the beam, but falling off: 3; and falling off the beam with no attempt to balance or hang on: 4.

Limb Placing Test

The limb placing test examines sensorimotor integration in limb placing responses to visual, tactile, and proprioceptive stimuli and was performed as described previously (18). A proprioceptive adduction test (18) was also performed. For each test, scoring was based on the following criteria: immediate and complete placing of the limb: a score of zero; incomplete and/or delayed (>2 seconds) placing, including interspersed flailing: one; and no placing: 2. Visual, forward tactile, and lateral tactile proprioceptive stimuli were given to the right forelimb. Forward tactile and lateral tactile and proprioceptive stimuli were given to the right hindlimb. Proprioceptive adduction tests were performed for both forelimb and hindlimb. The total score ranged from zero to 18.

Morris Water Maze Test

The Morris water maze test is a useful method to assess cognitive function (19, 20). Several modifications of this test have been reported; we refer readers to the work of Fukunaga et al (20). This test was performed from day 36 to day 40 after MCAO. A pool (diameter 150 cm, depth 35 cm) was prepared with an escape platform (diameter 10 cm) located 1 cm beneath the surface of the water, which was rendered opaque and milky white. Four starting points around the edge of the pool were designated as N, E, S, and W. The platform was kept in the middle of a particular quadrant, equidistant from the center and the edge of the pool. A rat was released into the

water from each starting point and allowed to swim until reaching the platform, and the time taken to reach the platform was recorded (maximum of 120 seconds). Rats were trained in the task using 2 sets of 4 trials on each of 5 consecutive days. After the first set on the fifth day, instead of the second set, a spatial probe trial was performed. This test is used to estimate short-term memory retention. The platform was removed and the rat was allowed to swim for 60 seconds. The number of times each animal crossed the area in which the platform had previously been located was measured (20). The time spent in the quadrant in which the platform had previously been located was also measured.

Histologic Analysis

The total period to finish the behavioral evaluation took one month after the cell transplantation. We intended to perform the histologic evaluation approximately one month after the transplantation. Therefore, we performed the histologic evaluation on day 41 from MCAO (34 days after the transplantation).

The rats were killed by administration of a pentobarbital overdose and then perfused transcardially with 0.9% saline followed by periodate-lysine-paraformaldehyde fixative solution (21). The brain was cut into coronal blocks of 2-mm thickness using Brain Matrix (BAS, Inc., Warwickshire, U.K.), and 10-μm-thick cryostat sections were made from each block. Sections were stained with hematoxylin and eosin to evaluate the infarct area. The images of sections were captured under a light microscope and the lesion areas were traced using Scion Image (Scion Corp., Frederick, MD). The infarct volume was calculated as described previously (22) and expressed as a percentage of the volume of the contralateral hemisphere.

For immunostaining, 14- to 16-μm cryosections were incubated with primary antibodies to MAP-2 (1:100; Boehringer Mannheim, Germany), β-tubulin-3 (1:400; Sigma), NF-M (1:200; Boehringer Mannheim), Tuj-1 (1:100; BAbCO, CA), or GFAP (1:400; Dako, Carpinteria, CA) at 4°C overnight. Alexa Fluor 546-conjugated anti-mouse IgG (Molecular Probes, Eugene, OR) (for MAP-2) or anti-rabbit IgG (Molecular Probes) (for β-tubulin-3, NF-M, Tuj-1, and GFAP) was used as the secondary antibody. TOTO-3 was used for nuclear staining. Specimens were inspected using confocal laser scanning microscopy (Radiance 2000; Bio-Rad, Hertfordshire, U.K.).

In each rat, the total number of GFP-labeled cells in the forebrain and hippocampus was determined. Ten sequential slides for each block were obtained and the mean number of GFP-labeled cells in each slide was measured. Because the approximate diameter of cell body of neuron is 20 μm (the cells less than 20 μm in diameter were excluded from the counting), we estimated the number of GFP-labeled cells in 2-mm-thick blocks could be obtained by multiplying the mean number of them by 100. The total number of GFP-labeled cells

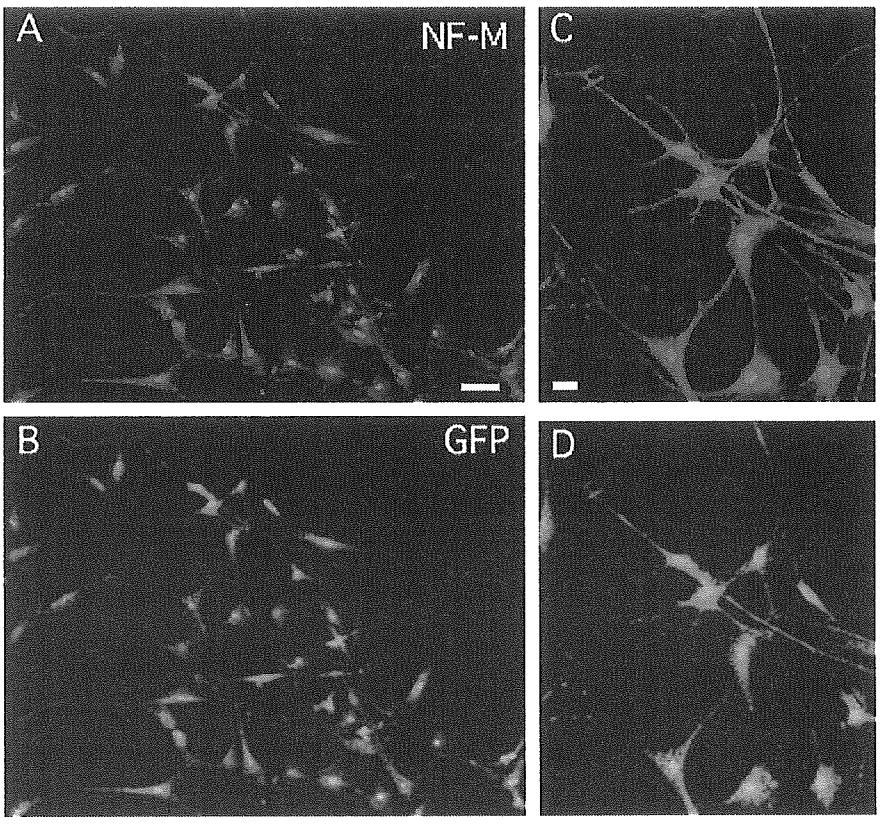

FIGURE 1. Confocal laser scanning microscopic images in vitro. Green fluorescent protein-labeled marrow stromal cell-derived neuronal cells (B, D) showed neurofilament-M positivity (A, C). Panels (A) and (B) are in lower magnification; panels (C) and (D) in higher magnification. Scale bars = (A, B) 50 μm; (C, D) 10 μm.

in the whole forebrain was then calculated by adding the numbers of GFP-labeled cells from all blocks. The number of GFP-labeled cells in the hippocampus was counted in the same way.

Statistical Analysis

The behavioral evaluation score and infarct volume are parametric data. For the statistical analysis among 3 groups, nonrepeated-measures analysis of variance was used. When the results were significant ($p < 0.05$), a Student-Newman-Keuls post hoc procedure was used at a 95% significant level using statistical software (Statistica StatSoft, Inc., Tulsa, OK). The values are presented as means ± standard deviation, unless otherwise stated.

RESULTS

The efficiency of retrovirus GFP introduction into MSCs was 98.0% ± 0.7%. The efficiency of NICD transfection was assessed by lipofection of pNICD-IRES2-EGFP, a GFP-containing plasmid, showing that 98.5% ± 0.8% of cells were transfected with NICD after G418 selection. MSDNCs induced from MSCs in vitro were subjected to the immunohistochemistry, showing that approximately 95% of GFP-labeled MSDNCs showed NF-M positivity and neurite extension consistent with a previous report (12) (Fig. 1). MAP-2ab and β-tubulin-3 showed similar results (data not shown).

One week after MCAO, and just before transplantation, severe right-sided neurologic deficits were apparent and the mean score for each behavioral test showed no statistical differences among the three groups. The results of behavioral analyses in the posttransplantation periods are summarized in Table 1 and Figures 2–5.

Beam Balance Test

From day 7 to day 21, the mean score was not statistically different among the 3 groups. On days 28 and 35, the mean score of the N-MSC group showed a significant improvement compared with the control (day 28: $p = 0.0041$, and day 35: $p = 0.0001$) and MSC groups ($p = 0.0471$ and 0.0007, respectively). Although the MSC group showed a slight improvement compared with the control group, a statistically significant difference could not be detected on days 28 and 35 (Table 1; Fig. 2).

Limb Placing Test

There were no statistical differences among the mean scores of the 3 groups from day 7 to day 21. On days 28 and 35, the N-MSC and MSC groups showed a significant improvement compared with the control group (day 28: $p = 0.0011$ and 0.0434, respectively, and day 35: $p = 0.0002$ and 0.0019, respectively). However, the mean score showed no significant difference between the N-MSC and MSC groups throughout the entire period (Table 1; Fig. 3).

Morris Water Maze Test

The mean latency time recorded in each set of 4 trials for location of the submerged escape platform is shown in Figure 4 for each of the 3 groups. The N-MSC group showed

TABLE 1. Results of Behavioral Analyses

	Mean ± Standard Deviation	p Value		
		Control	N-MSC	MSC
Beam balance test				
Day 28				
Control	2.28 ± 0.48		0.0041	0.1477
N-MSC	1.60 ± 0.51	0.0041		0.0471
MSC	2.00 ± 0	0.1477	0.0471	
Day 35				
Control	2.28 ± 0.48		0.0001	0.0652
N-MSC	0.8 ± 0.63	0.0001		0.0007
MSC	1.80 ± 0.42	0.0652	0.0007	
Limb placing test				
Day 28				
Control	13.71 ± 1.25		0.0011	0.0434
N-MSC	8.7 ± 2.35	0.0011		0.3293
MSC	9.9 ± 3.21	0.0434	0.3293	
Day 35				
Control	12.57 ± 1.39		0.0002	0.0019
N-MSC	7.8 ± 1.93	0.0002		0.1581
MSC	9.2 ± 2.39	0.0019	0.1581	
Morris water maze test				
Day 39 2*				
Control	86.39 ± 27.78		0.0339	0.376
N-MSC	38.97 ± 33.76	0.0339		0.0883
MSC	70.42 ± 44.70	0.376	0.0883	
Day 40 1†				
Control	75.96 ± 32.20		0.0492	0.5104
N-MSC	34.67 ± 26.65	0.0492		0.0787
MSC	64.95 ± 42.03	0.5104	0.0787	
Spatial probe trial				
Control	1.85 ± 2.03		0.0419	0.6438
N-MSC	5.4 ± 3.33	0.0419		0.0453
MSC	2.5 ± 2.83	0.6438	0.0453	
Spending time				
Control	13.57 ± 6.77		0.0339	0.4742
N-MSC	26.2 ± 10.96	0.0339		0.0628
MSC	17 ± 10.41	0.4742	0.0628	

*, Day 39 second set; †, Day 40 first set.

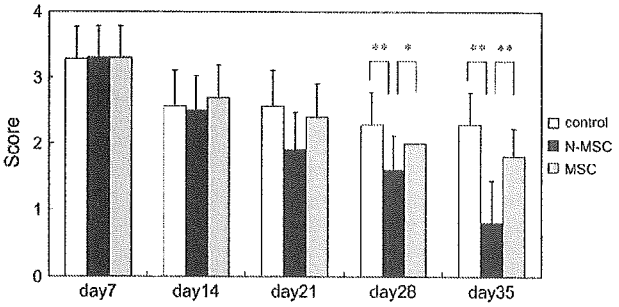

FIGURE 2. Beam balance test. On day 28 after transplantation, the mean score for the neuron induced from marrow stromal cell (N-MSC) group showed a significant improvement compared with the marrow stromal cell and control groups. *, $p = 0.05$, **, $p = 0.01$.

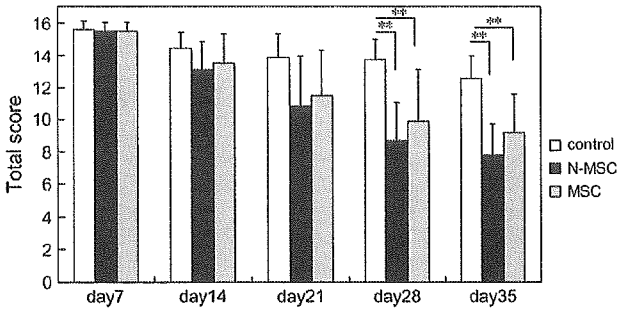

FIGURE 3. Limb placing test. The mean scores for the neuron induced from marrow stromal cell (N-MSC) group and the marrow stromal cell (MSC) group were significantly different to that of the control group on day 28 and day 35. There was no significant difference between the N-MSC and MSC groups. *, $p < 0.05$, **, $p < 0.01$.

a shorter latency time than the control and MSC groups. The mean latency time for the second set on day 39 and the first set on day 40 demonstrated a significant difference between the N-MSC and control groups ($p = 0.0339$ and 0.0492, respectively) (Table 1; Fig. 4). Although the N-MSC group showed a tendency for shorter times to find the escape platform compared with the MSC group, there was no statistically significant difference between the groups.

In the spatial probe trial, rats in the N-MSC group showed improvement compared with the control and MSC groups ($p = 0.0419$ and $p = 0.0453$, respectively) (Table 1; Fig. 5A). The mean time spent in the quadrant in which the platform had been located was longer in the N-MSC group compared with the control and MSC groups, and a statistical difference existed between the N-MSC and control groups ($p = 0.0339$) (Table 1; Fig. 5B).

Histologic Study

The infarct area was located in the lateral half of the left hemisphere, including the cortex, striatum, and hippocampus, and formation of cysts and scars was observed in many of the lesioned brains (Fig. 6). The hippocampus on the lesion side was atrophic and showed a partially irregular arrangement or loss of neurons compared with the contralateral side. Infarct volumes were measured in all MCAO models. The mean infarct volumes in the N-MSC, MSC, and control groups on day 33 were 50.7% ± 10.9%, 51.0% ± 10.2%, and 50.9% ± 11.1%, respectively. There was no statistically significant difference among the 3 groups.

Transplanted GFP-labeled MSCs and MSDNCs were located mainly at the boundary between intact tissue and the infarct area, including the ipsilateral cortex, corpus callosum, striatum, and hippocampus (Fig. 7A–F). Infiltration of inflammatory cells into the infarct focus was observed; however, the amount of inflammatory cells in the N-MSC and MSC groups was not significantly different. In the necrotic cyst in the ischemic hemisphere, many large GFP-labeled cells, which had large or multinuclei and had no neurites were observed. Because these cells appeared to be microglia and/or macrophages but not neurons or glial cells, we excluded these cells from the cell count.

Some of confocal microscopic images showed GFP signals as vesicular appearance (Fig. 7 I, J, L, M). This is probably because GFP was introduced as retrovirus and the fluorescence was not homogenously intense as usually observed in transgenic animal-derived cells. In fact, in our previous report (14), we demonstrated that GFP introduced with the retrovirus system in MSCs showed immunoelectron microscopic localization of GFP in association with membranes and vesicles in the cytoplasm, occasionally observed as patchy.

A large number of GFP-labeled MSDNCs were immunopositive for MAP-2 and showed neurite development in the host brain (Fig. 7G, H). These cells were also immunopositive for Tuj-1 and β-tubulin-3 (Fig. 7I, J). In the ipsilateral hippocampus, many cell bodies and neurites of GFP-labeled MSDNCs were also NF-M-positive (Fig. 7K–M). A large fraction of GFP-labeled transplanted MSDNCs were positive for MAP-2 (84.0% ± 8.1%), whereas only a small number of cells were positive for GFAP (1.0% ± 0.2%) (Fig. 7N).

In contrast, the large majority of MSCs in the host brain were negative for both neuronal (MAP-2, Tuj-1, β-tubulin-3, and NF-M) and glial (GFAP) markers (data not shown). The percentages of MAP-2- and GFAP-positive cells among the

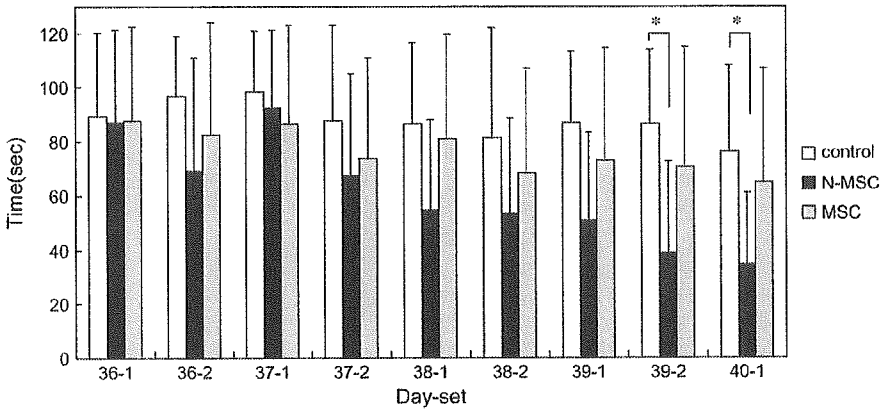

FIGURE 4. Morris water maze test. For the final set, the mean latency time for the neuron induced from marrow stromal cell (N-MSC) group was significantly different from those for the marrow stromal cell and control groups. *, $p < 0.05$.

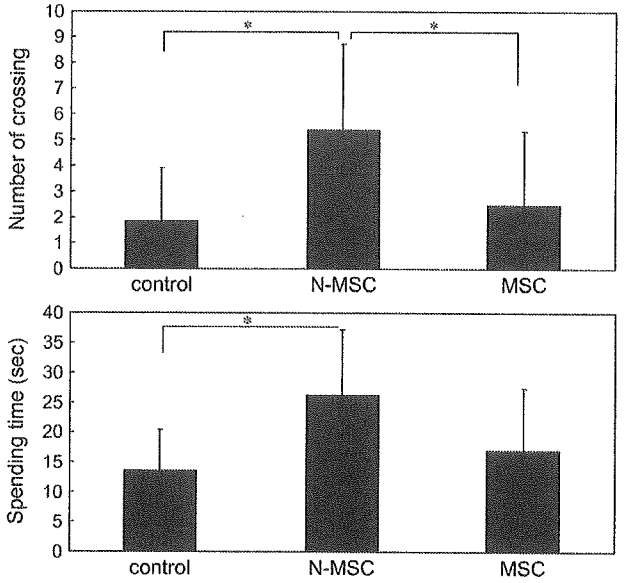

FIGURE 5. Water maze "spatial probe trial." Upper panel: the number of times the rat swam through the area in which the platform had previously been located. Lower panel: the time spent in the quadrant in which the platform had been located. Among the 3 groups, the best results were obtained for the neuron induced from marrow stromal cell (N-MSC) group, and statistical differences were obtained between the N-MSC group and the other groups. *, $p < 0.05$.

GFP-labeled cells were 1.4% ± 0.2% and 4.8% ± 1.0%, respectively. However, formation of neurites in MAP-2-positive MSCs could not be found.

The number of MSDNC in the host forebrain one month after transplantation ranged from 11,920 to 14,990 (the mean was 13,250 ± 1,126). The number of MSCs in the host forebrain ranged from 4,230 to 7,560 (the mean was 5,850 ± 997). Approximately 30% to 45% of the transplanted MSDNCs were detected, whereas only 10% to 20% of transplanted MSCs were detected. Thus, the survival rate of MSDNCs in the ischemic brain was substantially higher than that for MSCs. In the hippocampus, the number of MSDNC ranged from 610 to 980 (the mean was 790 ± 160) and 89% of these cells were MAP-2-positive. The number of MSCs, in contrast, ranged from 380 to 554 (the mean was 470 ± 66) and only 0.6% was MAP-2-positive, showing that most transplanted MSCs were negative for both neuronal and glial markers. In all 3 groups, no tumor formation in the brain parenchyma was observed up to 41 days after MCAO.

DISCUSSION

The N-MSC group showed significant improvements in the behavioral assessment tests compared with the control and MSC groups. In histologic analysis, the infarct volume determined at 41 days after MCAO did not show a significant difference among the 3 groups, suggesting that both MSDNC and MSC transplantation performed 7 days after MCAO had little effect on tissue protection. However, compared with MSCs, transplanted MSDNCs demonstrated a higher survival rate in the host brain and a larger proportion of MSDNCs were positive for neuronal markers, which might have contributed

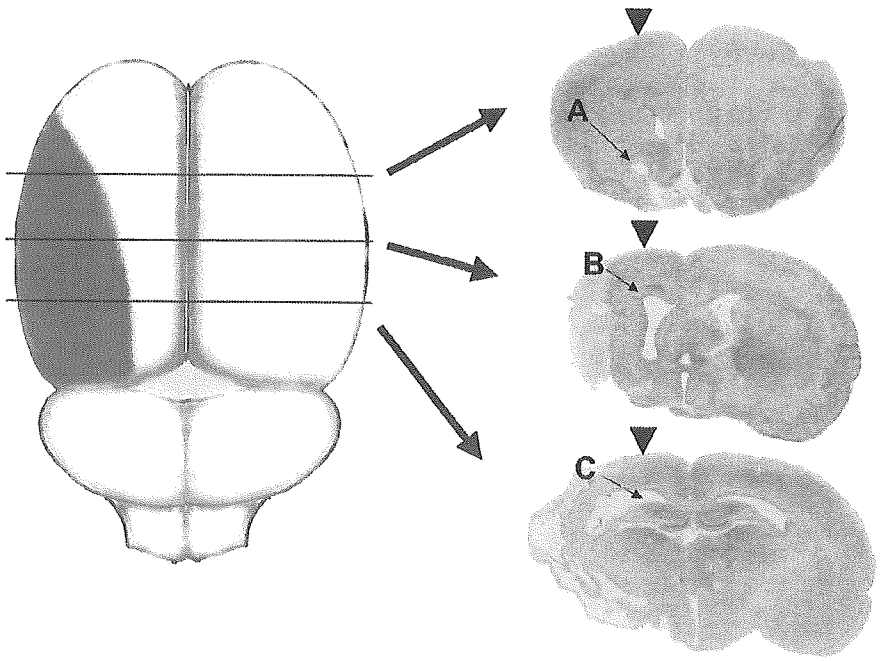

FIGURE 6. The drawing shows an image of the brain viewed from the upper side. The infarct area is shown in gray. Crossing lines are positioned 4, 6, and 8 mm from the pole of the frontal lobe. Color images show stained coronal sections of an infarcted brain from the neuron induced from marrow stromal cell (N-MSC) group (day 41). Arrowheads indicate the grafted sites on day 7. The characters and arrows correspond to the area indicated in Figure 7. Formation of necrotic cysts or scars was observed.

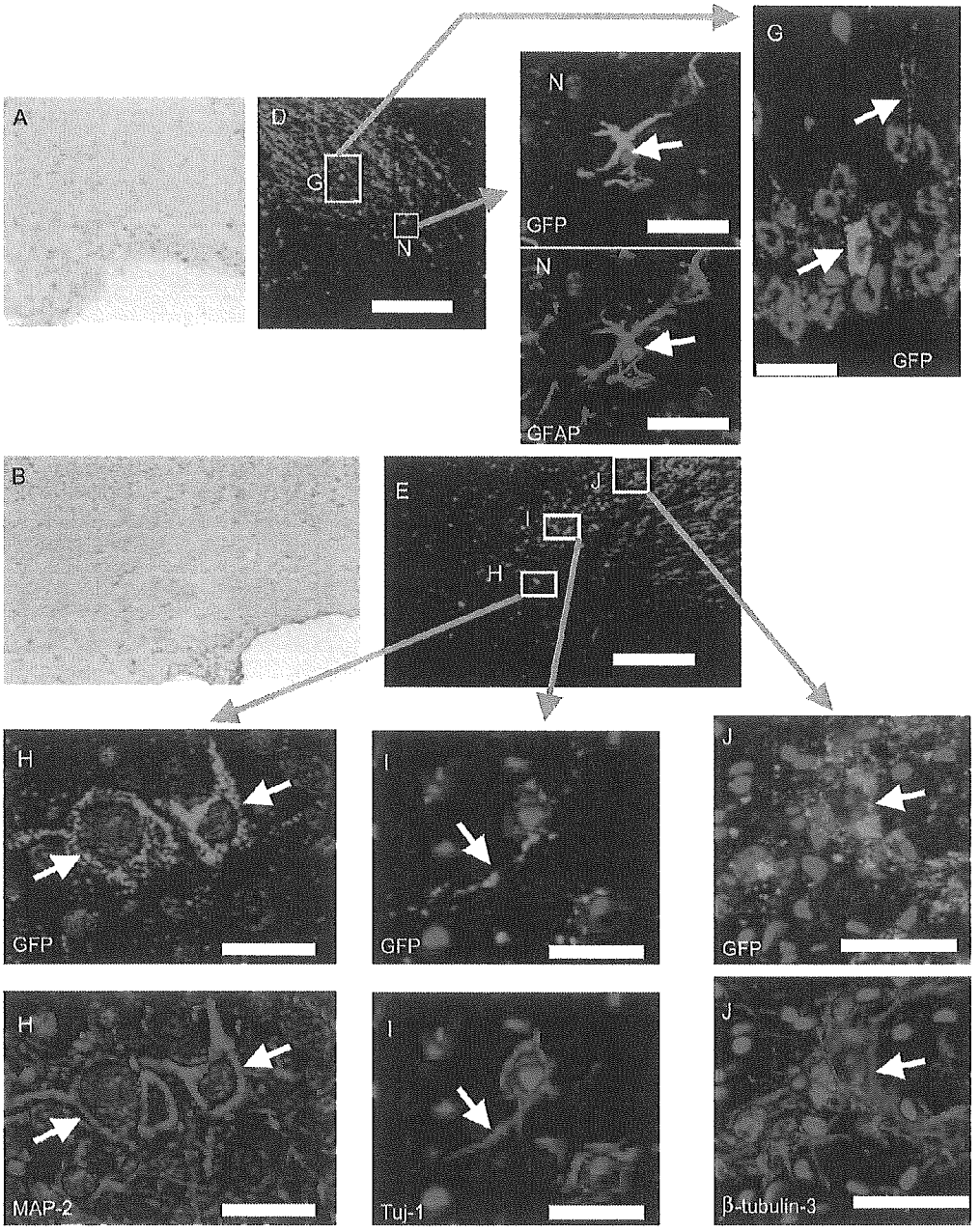

FIGURE 7. Histology of the infarcted brain in the neuron induced from marrow stromal cell (N-MSC) group on day 41. **(A–C)** Light microscopic images (low magnification) stained with hematoxylin and eosin. **(D–F)** Fluorescent microscopic images of the same areas shown in panels **(A–C)**, respectively. Green fluorescent protein (GFP)-labeled cells were observed in panels **(D–F)**. Scale bars = 200 μm. Squares correspond to the following LSCM images. **(G–N)** Tuj-1, MAP-2, β-tubulin-3, neurofilament-M (NF-M), and GFAP were labeled with Alexa546 (red color-coded), and nuclei were labeled with TOTO-3 (blue color-coded). Scale bars = 20 μm. **(G)** Transplanted marrow stromal cell-derived neuronal cells (MSDNCs) cell body and neurites were recognized as GFP-positive signals (arrows). **(H)** MAP-2-positive GFP-labeled MSDNCs were detected (arrows). **(I, J)** GFP-labeled cells were immunopositive for Tuj-1 **(I)** and β-tubulin-3 **(J)**. Arrows indicate GFP-positive cell bodies and neurites that were simultaneously positive for Tuj-1 and β-tubulin-3. **(K)** GFP-labeled cells expressing MAP-2 (arrows) were detected in the hippocampus of the ipsilateral hemisphere. **(L, M)** In the hippocampus of the ipsilateral hemisphere, GFP-labeled cells were immunoreactive to NF-M (arrows and arrowheads), and neurite extension was observed in these cells. **(N)** A small number of GFP-labeled cells showed GFAP positively.

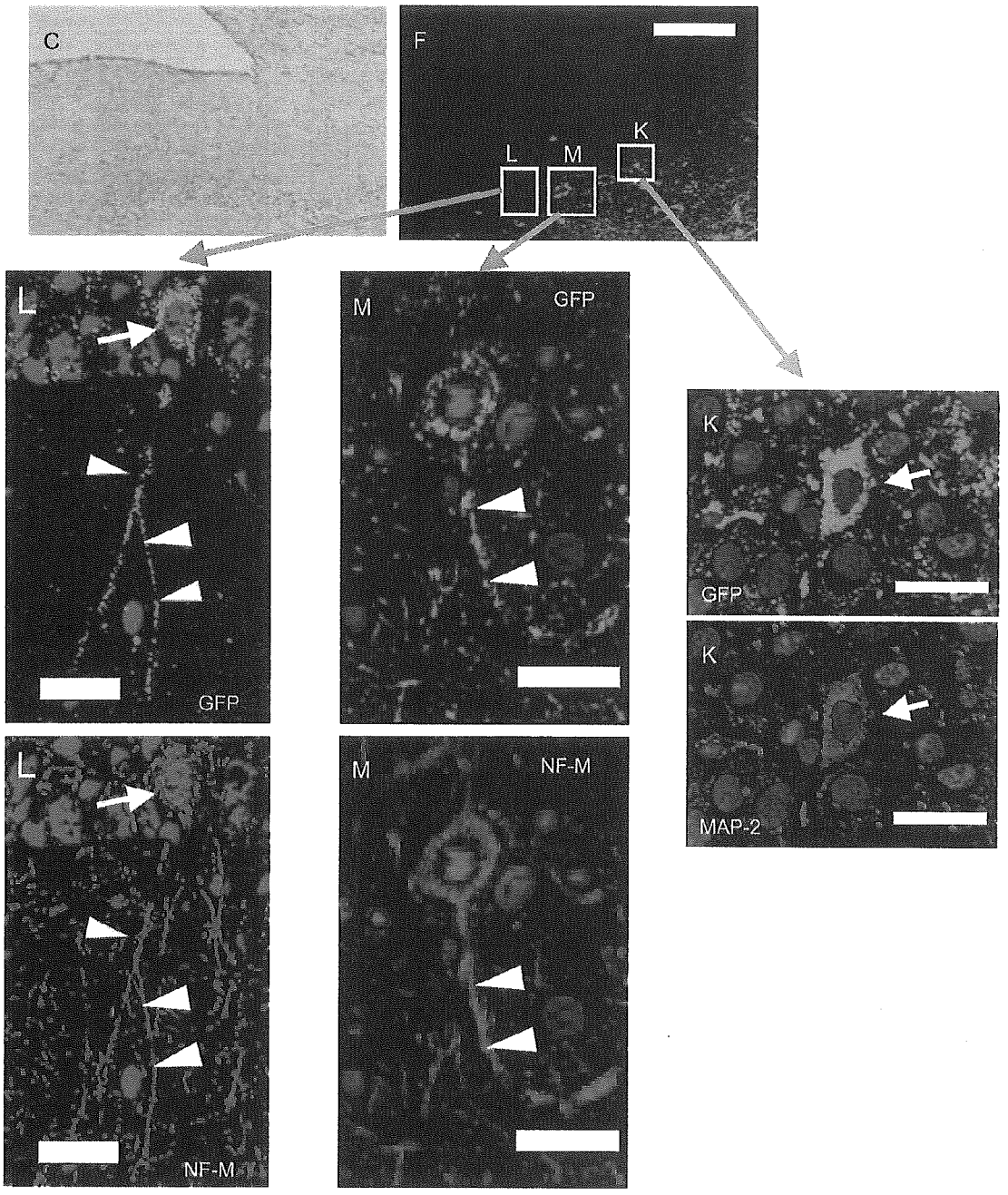

FIGURE 7. (*continued*).

to the improvements in the behavioral analysis. These results suggest that MSDNCs induced in vitro followed by transplantation is more effective than direct transplantation of nontreated MSCs.

As to the Notch protein expression in MSDNCs, NICD expression, which was clearly positive after transfection, gradually decreased according to the time course after neuronal induction, both in Western blot and reverse transcriptase–polymerase chain reaction (data not shown), is consistent with our previous report (12). This is probably the result of the degradation of introduced NICD, because NICD was introduced as plasmid DNA. These results suggest that NICD is necessary for the triggering neuronal induction in MSCs; however, once MSCs have acquired neuron-like characteristics,

NICD action is no longer necessary for maintaining their characteristics.

Notch-Hes signaling is known to inhibit neuronal differentiation and instructs glial differentiation in conventional neural development (23). However, in our system, NICD introduction accelerated the induction of neuronal cells from MSCs. Although our results appear inconsistent with previous work, they do not refute the known role of Notch-Hes signals in neurogenesis. In our previous report, JAK/STAT inhibitor administration and constitutive active STAT1/3 transfection showed that downregulation of STATs was tightly associated with NICD-mediated neuronal induction, whereas Hes, downstream of Notch, was not involved in the induction event (12). Thus, our results suggest distinct cellular responses to Notch signals; for example, the repertoire of second messengers and active factors may well be different between conventional neural stem cells and/or neural progenitor cells and MSCs. It might be possible that unknown signaling pathways downstream of Notch may be involved in these events, and thus further studies are needed to identify the factor(s) involved in this phenomenon.

The MSC group demonstrated slight improvements in behavioral assessment tests compared with the control group, but these improvements were not as significant as those for the N-MSC group. According to recent reports, MSC transplantation into the ischemic brain does lead to improvement of behavioral outcome. However, the survival rate of MSCs in the host brain was below 10%, and the proportion showing neuronal differentiation was only 1% to 2% (24–26). The functional recovery in behavior after MSC transplantation is thought to be mediated by neurotrophic factors produced by MSCs or by intrinsic parenchymal cells stimulated by MSCs (24–26).

In the current study, some MSDNCs in the cortex, striatum, and hippocampus demonstrated neurite extension in the host brain, which was not observed in the MSC-transplanted rats. Hence, the significant behavioral improvements in the N-MSC group suggest the transplanted MSDNCs maintained neuronal characteristics in the host brain and contributed to functional recovery in the MCAO rat model. However, positive effects associated with trophic factors produced by transplanted MSDNCs may also be present.

The potential of other kinds of stem cells such as NSCs and umbilical cord blood cells for use in ischemic brain injury has been reported recently (27, 28). Toda et al reported that engraftment of NSCs into a hippocampus damaged by transient global ischemia results in the partial improvement of impaired spatial learning in a water maze test (27). However, only 1% to 3% of the grafted cells survived and only 3% to 9% of these expressed NeuN. Chen et al reported that intravenous administration of human umbilical cord blood cells (HUCBCs) reduces behavioral deficits after stroke in rats (28). HUCBCs contain many stem and progenitor cells, although the percentage of HUCBCs that expressed NeuN, MAP-2, and GFAP was $\leq$2%, $\leq$3%, and $\leq$6%, respectively. In addition, approximately only 1% to 2% of intravenously injected HUCBCs were detected in the brain. In our study, 30% to 45% of MSDNCs survived in the host brain in the N-MSC group one month after transplantation and 84% of these cells expressed neuronal markers. In our experiment, neuronal differentiation itself seemed to contribute to the cell survival in the injured brain. Although because MSDNCs had received NICD transfection followed by the G418 selection, these manipulations might select a more robustly surviving subgroup from the original culture of MSCs. In addition, by using our retrovirus introduction system, GFP expression appeared to be maintained for a longer period after transplantation. These factors might have contributed to the higher survival rate in our study. Despite these facts, both NSCs and HUCBCs are very promising sources for donor cells. However, NSCs must be harvested from adult or fetal brain, which may have associated ethical problems, and long periods, on a clinical scale, are required for proliferation of NSCs. Although HUCBCs are widely available and have already been used clinically, further investigation is necessary to assess their efficacy for ischemic stroke.

In comparison to these cell types, MSCs are good candidates in that they can easily be obtained from patients or a bone marrow bank and they can be expanded in culture with fewer ethical problems. Furthermore, autologous transplantation of MSCs or transplantation of MSCs with the same HLA subtype from a healthy donor may minimize the risk of rejection. Aging is associated with a decreased maximal lifespan and accelerates senescence of MSCs, so that the MSDNC induction ratio may be variable according to the age of source. We estimated the influence of age (6-, 8-, and 12-week-old rats) in the MSDNCs induction. The ratio was basically similar among these ages and statistical differences could not be recognized (data not shown). Nonetheless, aging should be taken into account as one of the factors affecting transplantation.

For the clinical application of the cell transplantation therapy for the injured brain, transvenous or intrathecal cell injection is preferable because it is less invasive. In the current study, we performed direct intraparenchymal injection of MSDNCs because other methods include the uncertainty of cell distribution into the ischemic brain, which influence the evaluation of donor cell's survival rate.

The results presented here suggest that our method of specific induction of neuronal cells from MSCs has great potential in MSC transplantation therapy for neurologic disorders. However, further studies are needed to ensure the long-term safety and efficacy of manipulated MSCs.

REFERENCES

1. Zhang RL, Zhang ZG, Zhang L, et al. Proliferation and differentiation of progenitor cells in the cortex and the subventricular zone in the adult rat after focal cerebral ischemia. Neuroscience 2001;105:33–41
2. Aihara N, Mizukawa K, Koie K, et al. Striatal grafts in infarct striatopallidum increase GABA release, recognize GABAa receptor and improve water maze learning in the rat. Brain Res 1994;33:483–88
3. Goto S, Yamada K, Yoshikawa M, et al. GABA receptor agonist promotes reformation of the striatonigral pathway by transplant derived from fetal striatal promordia in the lesioned striatum. Exp Neurol 1997;147:503–9
4. Umezawa A, Maruyama T, Segawa K, et al. Multipotent marrow stromal cell line is able to induce hematopoiesis in vivo. J Cell Physiol 1992;151: 197–205
5. Makino S, Fukuda K, Miyoshi S, et al. Cardiomyocytes can be generated from marrow stromal cells in vitro. J Clin Invest 1999;103:697–705

6. Ferrari G, Cusella-De Angelis G, Coletta M, et al. Muscle regeneration by bone marrow-derived myogenic progenitors. Science 1998;279:1528–30
7. Kohyama J, Abe H, Shimazaki T, et al. Brain from bone: Efficient 'meta-differentiation' of marrow stroma-derived mature osteoblasts to neurons with Noggin or a demethylating agent. Differentiation 2001;68:235–44
8. Orlic D, Kajstura J, Chimenti S, et al. Bone marrow cells regenerate infarcted myocardium. Nature 2001;410:701–5
9. Woodbury D, Schwarz EJ, Prockop DJ, et al. Adult rat and human bone marrow stromal cells differentiate into neurons. J Neurosci Res 2000;61: 364–70
10. Sanchez-Ramos JR. Neural cells derived from adult bone marrow and umbilical cord blood. J Neurosci Res 2002;69:880–93
11. Jiang Y, Jahagirdar BN, Reinhardt RL, et al. Pluripotency of mesenchymal stem cells derived from adult marrow. Nature 2002;418:41–49
12. Dezawa M, Kanno H, Hoshino M, et al. Specific induction of neuronal cells from bone-marrow stromal cells and application for autologous transplantation. J Clin Invest 2004;113:1701–10
13. Azizi SA, Stokes D, Augelli BJ, et al. Engraftment and migration of human bone marrow stromal cells implanted in the brains of albino rats—similarities to astrocyte grafts. Proc Natl Acad Sci U S A 1998;95:3908–13
14. Dezawa M, Takahashi I, Esaki M, et al. Sciatic nerve regeneration in rats induced by transplantation of in vitro differentiated bone-marrow stromal cells. Eur J Neurosci 2001;14:1771–76
15. Koizumi J, Yoshida Y, Nakazawa T, et al. Experimental studies of ischemic brain edema. 1. A new experimental model of cerebral embolism in rats in which recirculation can be introduced in the ischemic area. Jpn J Stroke 1986;8:1–8
16. Longa EZ, Weinstein PR, Carlson S, et al. Reversible middle cerebral artery occlusion without craniectomy in rats. Stroke 1989;20:84–91
17. Dixon CE, Lyeth BG, Povlishock JT, Young HF, Hayes RL, et al. A fluid percussion model of experimental brain injury in the rat. J Neurosurg 1987;67:110–19
18. De Ryck M, Van Reempts J, Borgers M, et al. Photochemical stroke model: Flunarizine prevents sensorimotor deficits after neocortical infarcts in rats. Stroke 1989;20:1383–90
19. Morris RGM. Spatial localization does not require the presence of local cues. Learn Motiv 1981;12:239–60
20. Fukunaga A, Uchida K, Hara K, et al. Differentiation and angiogenesis of central nervous system stem cells implanted with mesenchyme into ischemic rat brain. Cell Transplant 1999;8:435–41
21. McLean IW, Nakane PK. Periodate-lysine-paraformaldehyde fixative. A new fixation for immunoelectron microscopy. J Histochem Cytochem 1974;22:1077–83
22. Swanson RA, Morton MT, Tsao-Wu G, et al. A semiautomated method for measuring brain infarct volume. J Cereb Blood Flow Metab 1990;10: 290–93
23. Lundkvist J, Lendahl U. Notch and the birth of glial cells. Trends Neurosci 2001;24:492–94
24. Chen J, Li Y, Wang L, et al. Therapeutic benefit of intravenous administration of bone marrow stromal cells after cerebral ischemia in rats. Stroke 2001;32:1005–11
25. Li Y, Chopp M, Chen J, et al. Intrastriatal transplantation of bone marrow non-hematopoietic cells improves functional recovery after stroke in adult mice. J Cereb Blood Flow Metab 2000;20:1311–19
26. Zhao LR, Duan WM, Reyes M, et al. Human bone marrow stem cells exhibit neural phenotypes and ameliorate neurological deficits after grafting into the ischemic brain of rats. Exp Neurol 2002;174: 11–20
27. Toda H, Takahashi J, Iwakami N, et al. Grafting neural stem cells improved the impaired spatial recognition in ischemic rats. Neurosci Lett 2001;316:9–12
28. Chen J, Sanberg PR, Li Y, et al. Intravenous administration of human umbilical cord blood reduces behavioral deficits after stroke in rats. Stroke 2001;32:2682–88

Neuron, Vol. 47, 201–213, July 21, 2005, Copyright ©2005 by Elsevier Inc. DOI 10.1016/j.neuron.2005.06.007

Ptf1a, a bHLH Transcriptional Gene, Defines GABAergic Neuronal Fates in Cerebellum

Mikio Hoshino,[1,2,11,*] Shoko Nakamura,[1,11] Kiyoshi Mori,[3,6] Takeshi Kawauchi,[1] Mami Terao,[1] Yoshiaki V. Nishimura,[1] Akihisa Fukuda,[4,5] Toshimitsu Fuse,[10] Naoki Matsuo,[1,12] Masaki Sone,[1,2] Masahiko Watanabe,[9] Haruhiko Bito,[10] Toshio Terashima,[7] Christopher V.E. Wright,[8] Yoshiya Kawaguchi,[2,4] Kazuwa Nakao,[3] and Yo-ichi Nabeshima[1]

[1]Department of Pathology and Tumor Biology
Graduate School of Medicine
Kyoto University
Sakyo-ku, Kyoto 606-8501
Japan

[2]Precursory Research for Embryonic Science and Technology (PRESTO)
Japan Science and Technology Agency
Kawaguchi, Saitama 332-0012
Japan

[3]Department of Medicine and Clinical Science
Kyoto University Graduate School of Medicine
Sakyo-ku, Kyoto 606-8507
Japan

[4]Departmentof Surgery and Surgical Basic Science
Kyoto University Graduate School of Medicine
Sakyo-ku, Kyoto, 606-8507
Japan

[5]Department of Gastroenterology and Hepatology
Kyoto University Graduate School of Medicine
Sakyo-ku, Kyoto, 606-8507
Japan

[6]Department of Medicine
College of Physicians and Surgeons of Columbia University
New York, New York 10032

[7]Division of Anatomy and Neurobiology
Department of Neuroscience
Kobe University Graduate School of Medicine
Kobe, 650-0017
Japan

[8]Vanderbilt Developmental Biology Program
Department of Cell and Developmental Biology
Vanderbilt University School of Medicine
Nashville, Tennessee 37232

[9]Department of Anatomy
Hokkaido University School of Medicine
Sapporo 060-8638
Japan

[10]Department of Neurochemistry
University of Tokyo Graduate School of Medicine
Bunkyo-ku, Tokyo 113-0033
Japan

*Correspondence: mikio@lmls.med.kyoto-u.ac.jp

[11]These authors contributed equally to this work.

[12]Present address: Department of Cell Biology and Institute for Childhood and Neglected Diseases, The Scripps Research Institute, La Jolla, California 92037.

Summary

The molecular machinery governing glutamatergic-GABAergic neuronal subtype specification is unclear. Here we describe a cerebellar mutant, *cerebelless*, which lacks the entire cerebellar cortex in adults. The primary defect of the mutant brains was a specific inhibition of GABAergic neuron production from the cerebellar ventricular zone (VZ), resulting in secondary and complete loss of external germinal layer, pontine, and olivary nuclei during development. We identified the responsible gene, *Ptf1a*, whose expression was lost in the cerebellar VZ but was maintained in the pancreas in *cerebelless*. Lineage tracing revealed that two types of neural precursors exist in the cerebellar VZ: *Ptf1a*-expressing and -nonexpressing precursors, which generate GABAergic and glutamatergic neurons, respectively. Introduction of *Ptf1a* into glutamatergic neuron precursors in the dorsal telencephalon generated GABAergic neurons with representative morphological and migratory features. Our results suggest that *Ptf1a* is involved in driving neural precursors to differentiate into GABAergic neurons in the cerebellum.

Introduction

Although a complex variety of neurons comprise the nervous system, they can be largely classified into two groups: excitatory and inhibitory neurons. In the central nervous system, these groups are mainly represented by glutamatergic and GABAergic neurons, respectively. In the rodent cerebral cortex, glutamatergic neurons are generated from the VZ of the dorsal telencephalon and migrate radially, while GABAergic neurons emerge from the ventral telencephalon and follow tangential migrations (Wilson and Rubenstein, 2000). Previous studies have suggested that a few basic helix-loop-helix (bHLH) transcriptional factors play a role in neuronal subtype specification in the telencephalon: neurogenins expressed in the dorsal telencephalon are involved in glutamatergic neuron production, and Mash1 in the ventral telencephalon participates in GABAergic neuron generation (Casarosa et al., 1999; Fode et al., 2000; Ross et al., 2003). These bHLH factors are localized in the VZ, where progenitors begin to differentiate, but not in the cortical plate, where mature neurons are located. However, the actual molecular machinery for specifying neuronal subtypes is still unclear and seems to be more complex, as suggested by recent studies that reported paradoxical results as well as the involvement of other types of transcriptional factors (Cheng et al., 2004; Parras et al., 2002; Schuurmans et al., 2004).

The cerebellum presents as a good model system for investigating the molecular mechanisms controlling neuronal subtype specification, because it contains only six or seven types of neurons, all of which are well characterized (Palay and Chan-Palay, 1974). The cerebellar VZ is known to generate different types of neu-

rons at distinct but overlapping developmental stages in mice (Wang and Zoghbi, 2001): deep cerebellar nuclei (DCN) neurons at embryonic day E10–E17, Purkinje cells at E11–E13, Golgi cells at E12–E15, and stellate/basket cells postnatally (Miale and Sidman, 1961; Pierce, 1975). While DCN neurons are known to include both glutamatergic (large cells) and GABAergic (small cells) populations (Batini et al., 1992), the other types of neurons are all GABAergic. This indicates that both glutamatergic (large DCN neurons) and GABAergic (Purkinje cells, Golgi cells, and small DCN neurons) neurons emerge from similar regions at overlapping stages, in contrast to the phenomenon in the telencephalon, where each type emerges from a distinct region. Despite the accumulated knowledge and simplicity of the cerebellum, the molecular machinery that governs GABAergic-glutamatergic neuronal subtype specification in the cerebellum is poorly understood.

Ptf1a (*pancreas transcription factor 1a*, also known as *Ptf1-p48*), which encodes a bHLH transcriptional factor, was originally reported as a pancreatic determiner that drives undifferentiated cells in the foregut endoderm to differentiate into a pancreatic lineage (Kawaguchi et al., 2002; Krapp et al., 1998). Very recently, *Ptf1a* was identified as a gene responsible for the human permanent neonatal diabetes mellitus associated with cerebellar ataxia and was reported to be somewhat involved in cerebellar development (Sellick et al., 2004).

Here we report that *Ptf1a* is expressed in the cerebellar VZ and acts as a neuronal subtype determiner to drive neural precursors in the cerebellar VZ to differentiate into GABAergic neurons. Loss of this gene expression results in a specific inhibition of GABAergic neuron production from the cerebellar VZ. Furthermore, introduction of this gene to glutamatergic neuron precursors in the dorsal telencephalon caused the production of neurons with GABAergic characteristics, in terms of not only the neurotransmitter subtype (GABA), but also cell morphology and migratory behavior. Surprisingly, our newly identified mutant, *cerebelless*, in which *Ptf1a* expression is lost in the cerebellum but maintained in the pancreas, survives up to adult lacking the entire cerebellar cortex.

Results

Phenotypes of *cerebelless* in Adults

During the generation of some transgenic mice, we obtained a line in which the homozygous mice exhibited tremor, ataxic gait, and uncoordinated locomotion in the adult stages (see Movie S1 in the Supplemental Data available online). Although they normally survived up to 2 years, their body sizes were generally smaller than those of heterozygotes and wild-type animals. Surprisingly, the brains of homozygotes seemed to lack the cerebellum (Figures 1A and 1B). Therefore, we named this mutant "*cerebelless*" (*cbll*). Hematoxylin-eosin (HE) staining of brain sections showed that the *cbll* mutant lacked all cerebellar cortical layers (Figures 1C–1F). In *Unc5h* mutant chimeras, ectopically localized cerebellar cells were found in the inferior colliculus (Goldowitz et al., 2000). However, no granule or Purkinje-like cells were observed outside the cerebellum in the *cbll* mutant as revealed by HE staining and immunohistochemistry (data not shown).

The *cbll* mutant brain retained a cerebellar rudimentary region that directly abutted the inferior colliculus (Figures 1E–1H). In this rudiment, DCN neuron-like cells were observed (Figures 1I and 1J), which were nonimmunoreactive to an anti-calbindin antibody (a marker for Purkinje cells, data not shown) but immunopositive to SMI32 antibody (Figures 1K and 1L), which supposedly labels both DCN neurons and Purkinje cells (Jankovski et al., 1996). Double labeling with SMI32 and anti-GABA antibodies of wild-type DCN showed a complementary staining pattern (Figure 1K); large cells were immunoreactive only to SMI32, and small cells were exclusively GABA positive. This suggests that SMI32 labels only glutamatergic neurons in the DCN, because large DCN neurons are known to be glutamatergic (Batini et al., 1992). In the mutant DCN, no GABA-positive cells were observed, although SMI32-positive neurons were found (Figure 1L). We performed immunostaining with an anti-glutaminase antibody that was reported to label glutamatergic DCN neurons (Kaneko et al., 1989) on wild-type and mutant DCNs and observed a considerable number of glutamatergic neurons even in the mutant DCN (Figures 1M and 1N). The number of large DCN cells, which are presumably glutamatergic neurons, was estimated by quantitation in serial sections (8272 ± 205 in the wild-type and 3461 ± 18 in *cbll*, n = 3). The number was significantly smaller in the mutant than in the wild-type ($p < 0.003$). Thus, our observations indicate that the GABAergic population of DCN neurons is completely absent in the *cbll* DCN, while loss of glutamatergic neurons is partial.

GABAergic neurons were missing within the entire mutant cerebellum, whereas many GABA-positive cells were found in other regions, such as the inferior colliculus (Figure 1O). As observed in Figures 1C and 1D, other than the cerebellum, the gross morphology of the mutant brain seemed normal. However, the inferior olivary nucleus and the pontine nuclei, which are known to project to the cerebellar cortex, were absent in adults (Figures 1P–1S).

cbll heterozygotes were normal at all developmental stages (data not shown).

Phenotypes of *cerebelless* during Development

During embryonic stages, the cerebellar primordium of the *cbll* mutant exhibited abnormal morphological features. At E14.5 and E16.5, although an external germinal layer (EGL)-like structure was observed in mutant embryos (Figures 2C and 2D, black arrowheads), the Purkinje cell layer was missing (Figure 2C, white arrowhead). At E14.5, newly born Purkinje cells can be labeled with an anti-calbindin antibody just above the VZ in wild-type embryos (Figure 2E); however, no calbindin-positive cells were observed in the mutant cerebellar primordium (Figure 2F), suggesting that Purkinje cells are not generated from the *cbll* cerebellar VZ. Our detailed immunohistochemical studies did not detect any calbindin-positive cells at any developmental stages in the *cbll* cerebellum (Figures 2E–2H and data not shown). In the wild-type cerebellum at E14.5 and

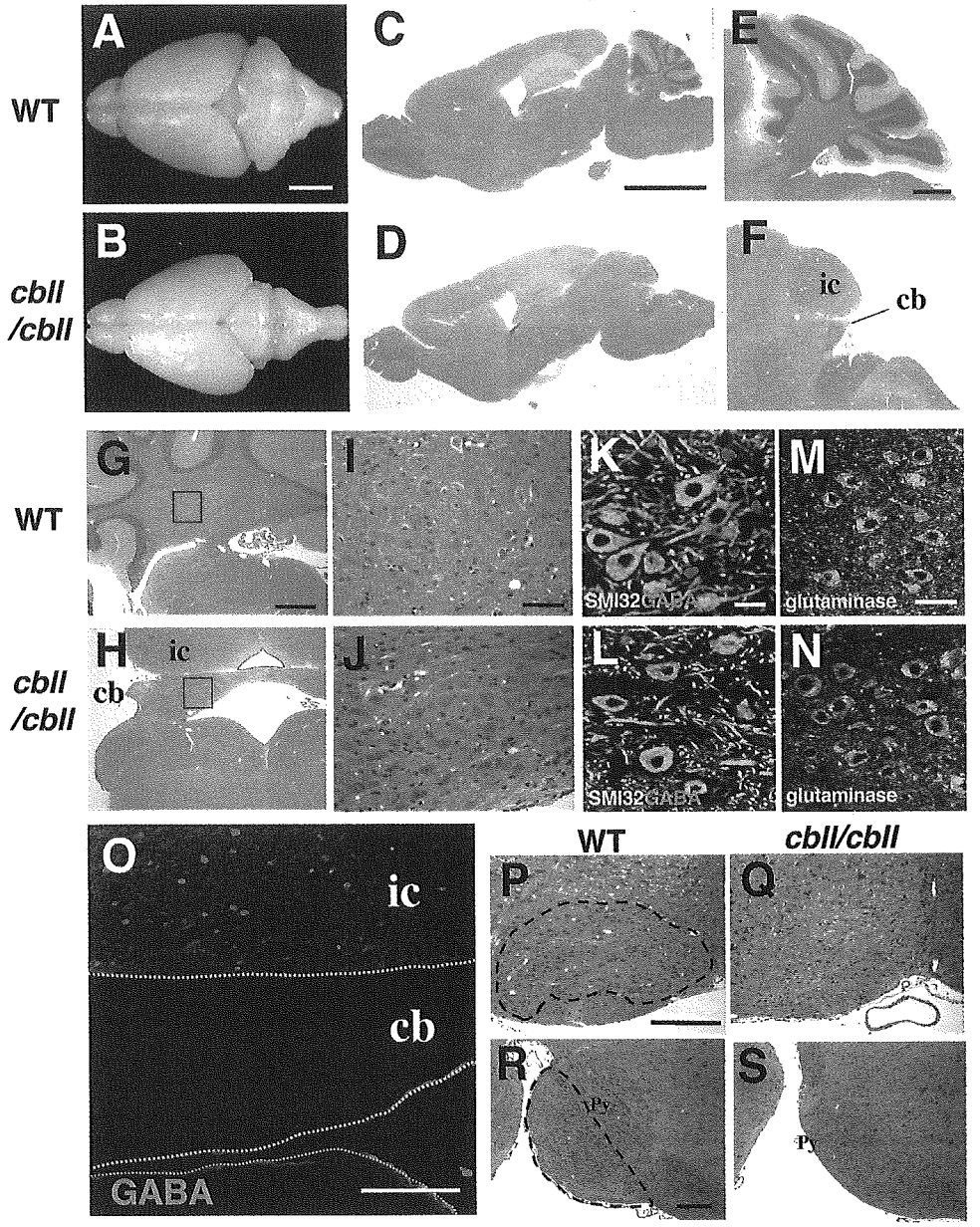

Figure 1. Adult Phenotypes of *cbll*

(A–F) Whole brains (A and B) and HE-stained sagittal sections (C–F) in adults. (G–O) Coronal sections of HE-stained (G–J) and immunostained (K–O) cerebella. (I and J) High-magnification images of the boxed areas in (G) and (H), respectively.

(K–N) DCN regions. (O) Low-magnification image of the cerebellar rudiment. Antibodies used are indicated. (P–S) Coronal and sagittal sections around the inferior olivary nucleus ([P and Q], surrounded by a dotted line) and the pontine nuclei ([R and S], surrounded by a dotted line). Genotypes are indicated. ic, inferior colliculus; cb, cerebellum; Py, pyramidal tract. Scale bars: (A–D) 3 mm, (E and F) 1 mm, (G and H) 500 μm, (I and J) 50 μm, (K and L) 20 μm, (M and N) 40 μm, (O–S) 200 μm.

E16.5, we observed many GABA-immunoreactive cells that likely include Purkinje cells, Golgi cells, and small GABAergic DCN neurons (Figures 2I and 2K). However, GABA-positive cells were rarely observed in the mutant cerebellum at these stages (Figures 2J and 2L), suggesting that GABAergic neurons were not produced from the VZ of the cerebellar primordium in *cbll*. In contrast, immunostaining with calretinin, a marker for a large population of differentiating DCN neurons at E14.5 (Jacobowitz and Abbott, 1998), revealed that a significant number of DCN neurons (probably glutamatergic) were generated in the mutant cerebellum. In situ hybridization with *Math1*, a marker for granule cell precursors (Ben-Arie et al., 1997), gave positive signals in the rhombic lip and the outer layer of the EGL at E12.5, E14.5 (data not shown), and E16.5 (Figures 2O–2R) in both wild-type and mutant animals, indicating that granule cell precursors were generated from the rhom-

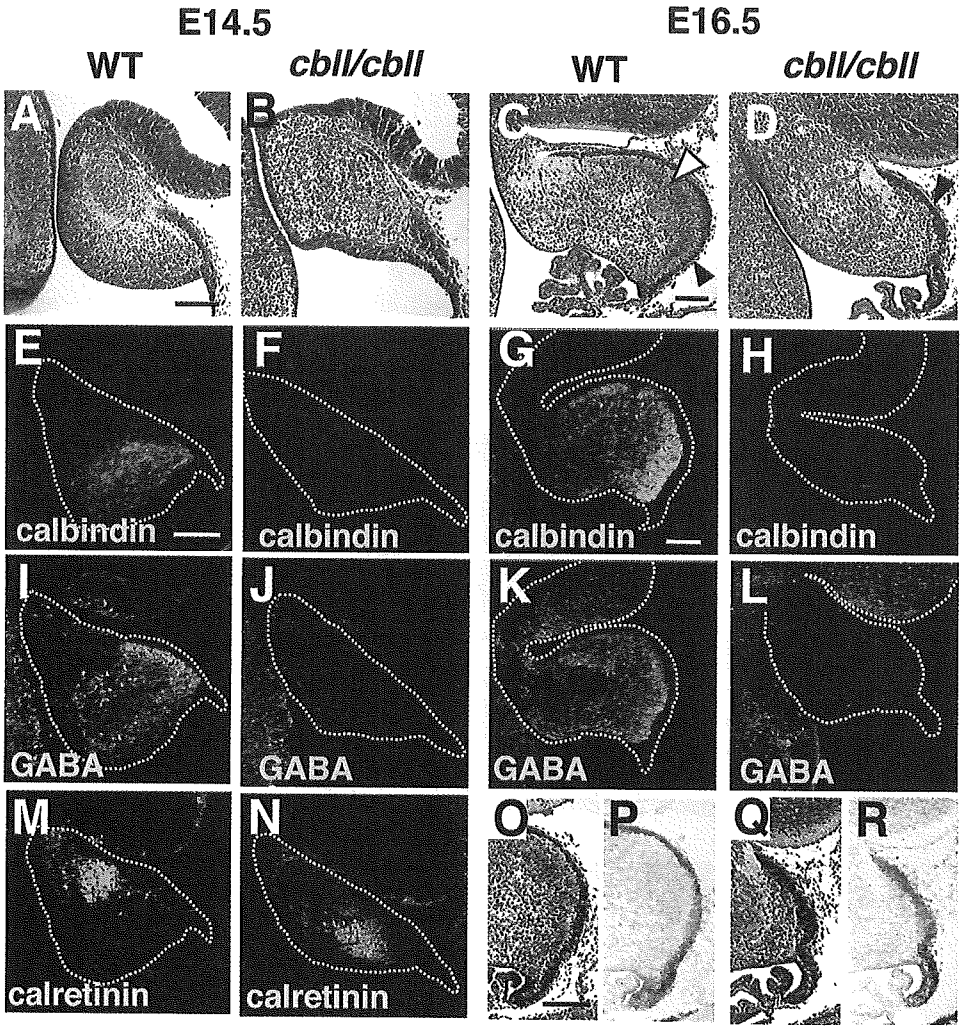

Figure 2. Cerebellar Phenotypes of *cbll* during Embryonic Development

(A–D) HE staining of sagittal sections of the cerebellar primordium. Black and white arrowheads indicate the EGL and Purkinje cell layers, respectively. Localization of calbindin (E–H), GABA (I–L), and calretinin (M and N) is shown. White dotted lines surround the cerebellar primordium. (O–R) In situ hybridization of cerebellar sections probed with *Math1* (P and R), accompanied with HE-stained serial sections (O and Q). Genotypes and developmental stages are indicated. Scale bars, 150 μm.

bic lip even in the *cbll* mutant. These findings suggest that generation of all types of GABAergic neurons was affected in the *cbll* cerebellar VZ, although glutamatergic neurons, namely, large DCN neurons, continued to be produced.

HE staining of postnatal samples revealed that, with the exception of the mutant cerebellum and inferior olivary and pontine nuclei, other regions of the brain were unaffected. At postnatal day 4 (P4), the mutant cerebellum was smaller and did not exhibit the characteristic lobular structure (Figures 3A and 3B). The Purkinje cell layer was absent, and the EGL was much thinner (Figures 3C and 3D), as confirmed by in situ hybridization with *Math1* (Figures 3E–3H). As development proceeded, the size of the mutant cerebellum decreased relative to that of the whole brain (Figures 3I and 3J). The EGL became smaller and thinner and disappeared by P7 (data not shown) and P14 (Figures 3K and 3L) in *cbll* mutants. Eventually, granule cells could hardly be found in the *cbll* cerebellum.

Interestingly, in the mutant, the inferior olivary and the pontine nuclei developed normally until P2 (Figures 3M and 3P) and P5 (Figures 3S and 3V), respectively. However, the inferior olivary nuclei started to regress at P4 (Figures 3N and 3Q) and disappeared by P6 (Figures 3O and 3R). Similarly, the pontine nuclei began to disappear at P6 (Figures 3T and 3W) and was barely distinguishable by P7 (Figures 3U and 3X).

TUNEL staining revealed many more apoptotic cells in the EGL at P0, the inferior olivary nucleus at P3, and the pontine nuclei at P6 in the mutants than in the wild-type mice (Figure S1). These phenomena indicate that granule cell precursors and neurons in the inferior olivary and pontine nuclei were initially generated in the

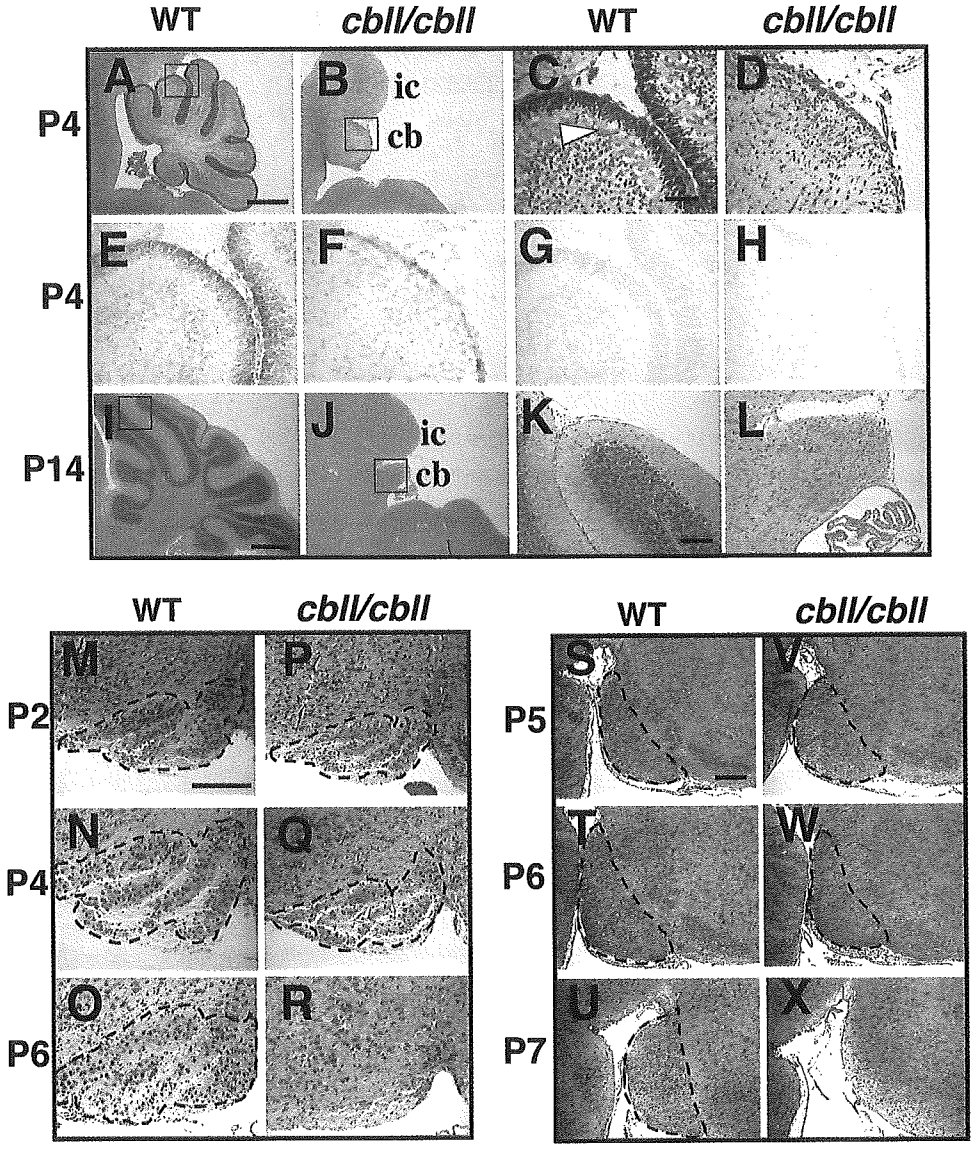

Figure 3. Postnatal Phenotypes of *cbll*

(A–D and I–L) HE sections of wild-type and mutant cerebella. A white arrowhead indicates the Purkinje cell layer. (E–H) In situ hybridization with *Math1* antisense (E and F) and sense (G and H) probes of adjacent sections of (C) and (D). Enlarged pictures in rectangles are shown (C, D, K, and L). (M–R) Inferior olivary nucleus (surrounded by a dotted line). (S-X), Pontine nuclei (surrounded by a dotted line). Genotypes and developmental stages are indicated. ic, inferior colliculus; cb, cerebellum. Scale bars, (A, B, I, and J) 500 μm, (C–H) 50 μm, (K and L) 100 μm, (M–X) 200 μm.

mutant but secondarily lost during development by apoptosis, in contrast to the GABAergic neurons in the *cbll* cerebellum.

Ptf1a Is the Responsible Gene for *cerebelless*

To identify the responsible gene for the *cbll* phenotype, we performed fluorescence in situ hybridization (FISH) analyses of the mutant chromosomes. The transgene (see Experimental Procedures) appeared to have been inserted into a single locus of chromosome 2, around regions 2A3–2B (Figures 4A and 4B). Our genetic linkage analyses indicated that the transgene was introduced between genetic markers D2Mit178 and D2Mit79 (Figure 4C). As the generation of transgenic mice is sometimes accompanied by a deletion of genomic sequences near the transgene insertion site (Kuro-o et al., 1997), we looked for possible genomic deletions between the two genetic markers. Using a series of primer pairs that could amplify small DNA fragments (~100 bp) from the wild-type genome but not from the genomic DNA of *cbll* homozygotes resulted in the successful identification of a 313 kb deletion in the *cbll* genome (Figure 4C). According to the NCBI mouse genome database, the *Ptf1a* gene, which encodes a bHLH tran-

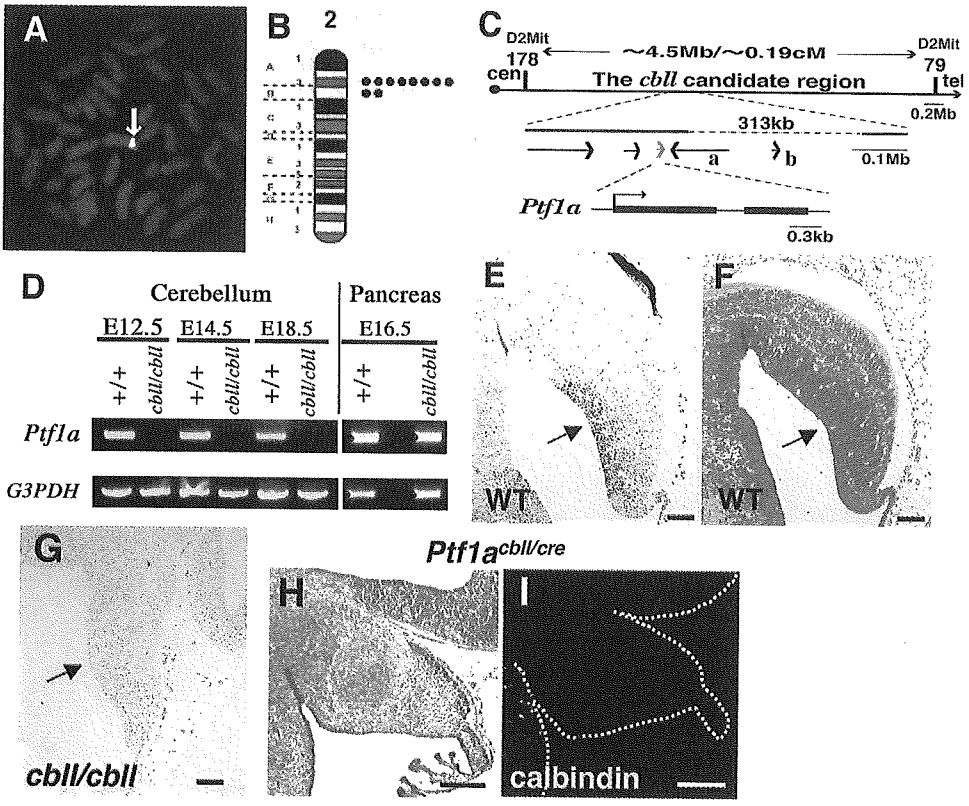

Figure 4. *Ptf1a* Is the Responsible Gene for *cbll*

(A and B) FISH analysis of *cbll* chromosomes probed with the transgene. (C) Physical/genetic map around the transgene insertion site. Arrows indicate distinct genes. *Ptf1a* (red arrow) and a 313 kb deletion are shown. Arrows a and b indicate the *4921522E24Rik* and *4933428L19Rik* genes, respectively. (D) RT-PCR to mRNA purified from cerebellum and pancreas at indicated stages. (E and G) In situ hybridization with *Ptf1a* to E12.5 cerebella. (F) HE staining of the adjacent section of (E). Arrows, ventricular side of the cerebellar primordium. (H and I) Adjacent frozen sections of the cerebellum of the transheterozygote ($Ptf1a^{cre/cbll}$) at E16.5 stained with HE (H) and calbindin (I). Scale bars, (E–G) 100 μm, (H and I) 200 μm.

scriptional factor, is located 60 kb from one end of the deletion (Figure 4C). Because *Ptf1a* was reported to be expressed not only in pancreas but also in the developing cerebellum (Obata et al., 2001), it was a good candidate for the responsible gene. RT-PCR of mRNAs purified from embryonic cerebellar primordium detected *Ptf1a* transcripts in wild-type embryos at E12.5, E14.5, and E18.5 (Figure 4D), but not in mutant embryonic cerebella at any stage (Figure 4D). On the other hand, *Ptf1a* was found to be expressed in both wild-type and mutant embryonic pancreas (Figure 4D). In situ hybridization of embryonic brains showed that *Ptf1a* is expressed in the ventricular region of the cerebellar primordium at E10.5, E12.5, and later stages (Figure 4E and data not shown), with little or no expression in the telencephalon (data not shown), in agreement with Obata et al. (2001). Comparison to HE-stained serial sections indicated that *Ptf1a* was expressed within the cerebellar VZ (Figure 4F). In *cbll* mutants, *Ptf1a* transcripts were not detected in the cerebellar primordium (Figure 4G), consistent with our RT-PCR data. Moreover, a transheterozygote of *cbll* and a *Ptf1a* null allele, $Ptf1a^{cre}$ ($Ptf1a^{tm1(cre)Wri}$) (Kawaguchi et al., 2002), exhibited abnormal cerebellar morphology at E16.5, lacking the Purkinje cell layer (Figure 4H). In an adjacent section, calbindin-positive cells were hardly observed in the cerebellum of the transheterozygote (Figure 4I). These phenotypes were basically identical to those of the *cbll* homozygote shown in Figure 2. The $Ptf1a^{cre/cre}$ null mutant also exhibited similar cerebellar defects with the *cbll* mutant at late embryonic stages (data not shown). These results support *Ptf1a* as being the responsible gene for the *cbll* phenotype and further suggest that *cbll* is one of the alleles of *Ptf1a* ($Ptf1a^{cbll}$), specifically affecting the cerebellar primordium, but sparing the developing pancreas. The null mutation of *Ptf1a* has been reported to result in pancreatic malformation and dysfunction as well as perinatal death from an unknown cause (Kawaguchi et al., 2002; Krapp et al., 1998). In contrast, the *cbll* mutant ($Ptf1a^{cbll/cbll}$) survives up to 2 years with a normal pancreas (data not shown).

Lineage Tracing of *Ptf1a*-Expressing Cells

The $Ptf1a^{cre}$ allele was generated by the replacement of the *Ptf1a* protein-coding region with that of a Cre recombinase targeted to the nucleus (Kawaguchi et al., 2002). We crossed $Ptf1a^{cre/+}$ with $Gt(ROSA)26Sor^{tm1sor}$ (*R26R*) mice, which carry a modified *lacZ* gene driven by the cell type-independent *ROSA26* promoter (Sori-

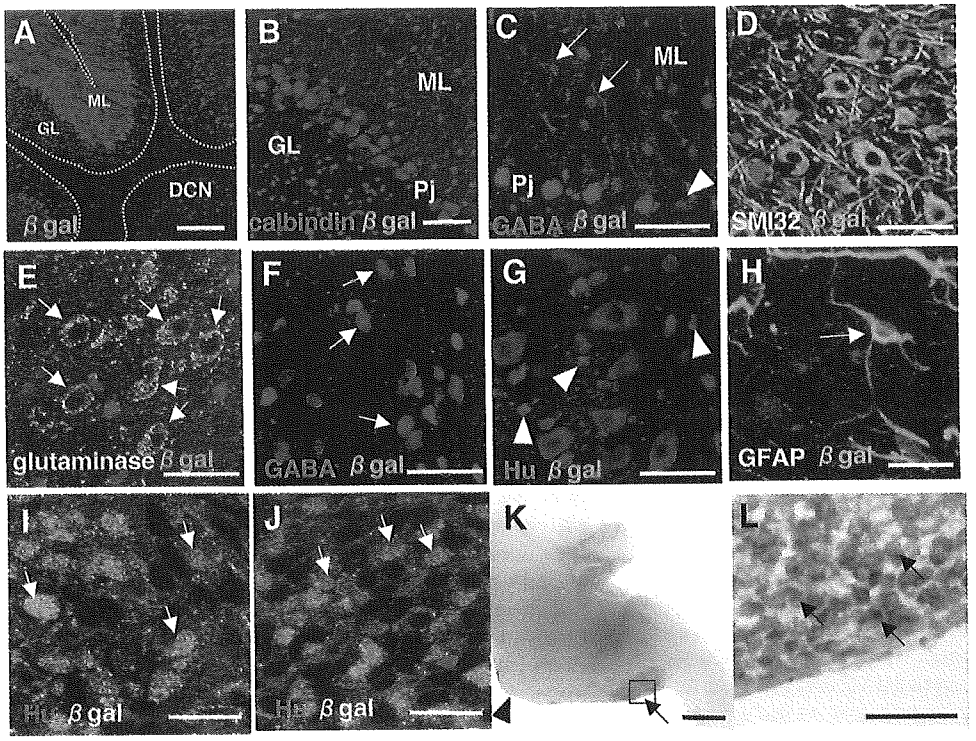

Figure 5. Lineage Tracing Analyses in the Cerebellum

(A–H) *Ptf1a*$^{cre/+}$;*R26R* cerebella at P30 stained with indicated antibodies. PJ, Purkinje cell layer; ML, molecular layer; GL, granular layer; DCN, deep cerebellar nuclei. (C) In the adult brain, neuronal soma of Purkinje cells are known to be hardly stained with GABA. An arrowhead and arrows indicate basket and stellate cells, respectively. (E) Arrows indicate glutamatergic neurons in the DCN. (I and J) Immunostaining with β-galactosidase and HuC/D to the cerebellar primordium of *Ptf1a*$^{cre/+}$;*R26R* (I) and *Ptf1a*$^{cre/cbll}$;*R26R* (J) at E14.5. Regions just above the cerebellar VZ. (K) A parasagittal slice of a X-gal-stained *Ptf1a*$^{cre/+}$;*R26R* brain at P0. The pontine nuclei (arrowhead) and the inferior olivary nucleus (arrow) are indicated. (L) Higher-magnification view of the rectangular region in (K), which was counterstained with 0.5% neutral red. Arrows indicate β-galactosidase-positive cells in the inferior olivary nucleus. Scale bars, (A) 200 μm, (B–G) 50 μm, (H–J) 20 μm, (K) 200 μm, (L) 40 μm.

ano, 1999). In offspring obtained from this cross, *Ptf1a*-driven expression of Cre excises a stop cassette upstream of *lacZ* and activates β-galactosidase expression, which eventually labels *Ptf1a*-expressing cells and their progeny (Kawaguchi et al., 2002).

Immunostaining revealed numerous β-galactosidase-positive cells in the adult cerebellum of the *Ptf1a*$^{cre/+}$;*R26R* mouse (Figure 5A). In the cerebellar cortex, β-galactosidase was expressed in many types of GABAergic neurons; Purkinje cells are shown by double labeling with calbindin (Figure 5B), stellate (Figure 5C, arrows), and basket (Figure 5C, arrowhead) cells by double labeling with GABA in the molecular layer and Golgi cells in the inner granular layer (data not shown). In the DCN, expression of β-galactosidase was detected only in small cells that were never labeled with SMI32, a marker for non-GABAergic large DCN neurons (Figure 5D) (Batini et al., 1992). Accordingly, glutaminase-positive cells (arrows in Figure 5E) in the DCN, which are glutamatergic neurons, were never labeled with β-galactosidase. In contrast, many β-galactosidase-expressing cells were GABA positive in the DCN (Figure 5F, arrows), indicating that *Ptf1a*-expressing precursor cells in the cerebellar VZ produced GABAergic but not glutamatergic neurons in the DCN. Some β-galactosidase-positive cells were not immunoreactive to HuC/D, a marker for postmitotic neurons (Figure 5G, yellow arrowheads), indicating that *Ptf1a*-expressing precursors also produced nonneuronal cells. This might account for the presence of the β-galactosidase-positive, GABA-negative cells in Figure 5F. Some β-galactosidase-positive cells were labeled with GFAP, a marker for astrocytes (arrow in Figure 5H). Similarly, it has been known that both neuronal and glial cells emerge from common precursors in the VZ of the dorsal telencephalon (Kriegstein and Gotz, 2003; Temple, 2001).

On the other hand, β-galactosidase-negative, calbindin-positive, or GABA-positive cells were also observed in Figures 5B and 5F. Transient and/or low expression of Cre often results in "escapers" in this "Cre-loxP" lineage trace system (Gu et al., 2002). Because Cre recombinase in *Ptf1a*$^{cre/+}$;*R26R* mice should be active only in the precursor cells in the cerebellar VZ but not in postmitotic neurons, early-born neurons are expected to include more escapers than late-born neurons. Actually, Purkinje cells and DCN neurons, which are known to be generated at embryonic stages, were sometimes β-galactosidase negative (Figures 5B and 5F), while most basket and stellate cells that are produced postnatally are β-galactosidase positive (Figure

5C). Therefore, the β-galactosidase-negative Purkinje and GABAergic DCN neurons detected in Figures 5B and 5F might be escapers generated from *Ptf1a*-expressing precursors. The fact that all types of GABAergic neurons were affected in the mutant also supported this notion.

The results of the lineage trace analyses suggest the existence of at least two types of neural precursor cells in the cerebellar VZ: *Ptf1a*-expressing precursors that produce a variety of GABAergic neurons and *Ptf1a*-nonexpressing precursors that generate glutamatergic DCN neurons.

The lineage trace analysis was also applied to E14.5 embryonic cerebellar primordium in the mutant background (*Ptf1a*$^{cre/cbll}$;*R26R*), in conjunction with HuC/D immunostaining. At this stage, HuC/D signals were found in cytoplasmic regions surrounding the nucleus, while β-galactosidase was detected in nuclear and/or perinuclear regions (arrows in Figure 5I). Many β-galactosidase-positive cells were found to be HuC/D positive, even in the mutant cerebellum (arrows in Figure 5J). Rates of HuC/D-expressing cells in β-galactosidase-positive cells were 95.05% ± 1.47% in control and 93.57% ± 4.60% in mutants. These facts indicate that neural precursors in the cerebellar VZ can produce neurons despite loss of *Ptf1a* expression. At the same developmental stage (E14.5), the positioning of β-galactosidase-positive cells was abnormal in the mutant (Figure S3). Some cells were found beyond the cerebellar primordium (arrow), and some were abnormally located facing the dorsal surface of the primordium (arrowhead). This observation may implicate that the migratory behavior of cells in the cerebellum is affected when they lose the *Ptf1a* expression. Furthermore, we performed the lineage trace analysis of neonatal cerebellum in the mutant background (*Ptf1a*$^{cre/cbll}$;*R26R*) with GFAP immunostaining, obtaining results showing that some β-galactosidase-expressing cells were GFAP positive (data not shown). This indicates that neural precursors in the cerebellar VZ can also produce astrocytes, even in the absence of *Ptf1a* expression.

To investigate whether proliferation of the β-galactosidase-positive cells in the cerebellar VZ was affected in the mutant background, pregnant mice (E12.5) were given two intraperitoneal injections of BrdU with a 30 min interval. One hour after the first BrdU injection, the embryos were fixed, and BrdU incorporation rates were estimated. BrdU incorporation rates of β-galactosidase-positive cells in the cerebellar VZ were 22.81% ± 3.38% in *Ptf1a*$^{cre/+}$;*R26R* and 22.21% ± 3.17% in *Ptf1a*$^{cre/cbll}$;*R26R* embryos, respectively (mean ± SEM, n = 7), indicating that proliferation of neural precursors in the cerebellar VZ is not significantly affected by loss of *Ptf1a* expression.

Interestingly, X-gal staining of P0 whole-mount brains of *Ptf1a*$^{cre/+}$;*R26R* mice revealed that the inferior olivary but not pontine nuclei are β-galactosidase positive (Figure 5K). In high-magnification pictures, many β-galactosidase-expressing cells were observed in the inferior olivary nucleus (Figure 5L), but not in the pontine nuclei (data not shown). Because *Ptf1a* is reportedly expressed in the dorsal part of the rhombencephalon (Obata et al., 2001), neurons in the inferior olivary nuclei may be derived from *Ptf1a*-expressing cells in the dorsal rhombencephalon.

Ptf1a Confers GABAergic Characteristics on Neurons Produced from the Dorsal Telencephalon

In rodents, it is known that the VZ of the dorsal telencephalon produces glutamatergic neurons that migrate radially, but does not generate GABAergic neurons that migrate tangentially (Wilson and Rubenstein, 2000). Therefore, we introduced this gene into the VZ of the dorsal telencephalon, where *Ptf1a* is not endogenously expressed, to examine whether the fates of the progeny neurons are changed. By using an in utero electroporation technique (Kawauchi et al., 2003), we cointroduced the *Ptf1a* expression (or a control) plasmid with an enhanced GFP expression vector into the VZ of the dorsal telencephalon at E14.5 and observed the resulting phenotypes at subsequent stages. The cotransfection efficiency was more than 98%, as previously described (Kawauchi et al., 2003). We confirmed that under our experimental conditions the expression plasmid was not introduced into ventral telencephalon cells by sacrificing and analyzing the animals 24 hr after electroporation (data not shown). At P0, frozen sections of electroporated brains were prepared and subjected to immunohistochemistry with anti-GABA and anti-GFP antibodies. In control animals, the majority of GFP-positive cells had migrated to the superficial layers of the cortical plate (Figure 6A), as previously described (Kawauchi et al., 2003). These transfected cells were not GABA positive (Figures 6C-6E), coincident with previous reports (Tan et al., 1998; Wilson and Rubenstein, 2000). In contrast, *Ptf1a*-transfected cells were found in various regions of the cortex, namely, all layers of the cortical plate, the intermediate zone, and even the marginal zone (Figure 6B), suggesting that these cells do not migrate normally. Surprisingly, *Ptf1a*-transfected cells in the upper (Figures 6F–6H) and lower layers (Figures 6I–6K) of the cortical plate were often immunoreactive to GABA. The ratios of GABA-positive cells to GFP-positive cells in the cortical plate were 75.053% ± 1.93% and 0.032% ± 0.032% in the *Ptf1a*-introduced and control brains, respectively ($n = 14$, $p < 0.0001$).

Furthermore, enhancement of the GFP signals showed that *Ptf1a*-transfected, GABA-positive cells tended to harbor multiple thin processes around the soma, resembling the morphology of typical GABAergic neurons in the cerebral cortex (Figures 6L and 6M). Similar phenomena were observed when the electroporated animals were sacrificed at E17.5. Many *Ptf1a*-introduced cells were GABA positive (see Figures S2A–S2F), and some cells resided in the marginal zone extending a process toward the ventricular side (Figure S2G), resembling a type of migratory behavior recently reported for GABAergic neurons (Ang et al., 2003). In the intermediate zone of brains sacrificed at P0, fewer *Ptf1a*-transfected cells were GABA positive, but many exhibited tangentially migrating GABAergic neuron-like morphology (Figures 6N–6P). To investigate the migratory behavior of *Ptf1a*-introduced cells, we performed time-lapse recording on cultured brain slices that were electroporated at E14.5 and sacrificed at E16.5. In contrast to the radial migration observed in most of the

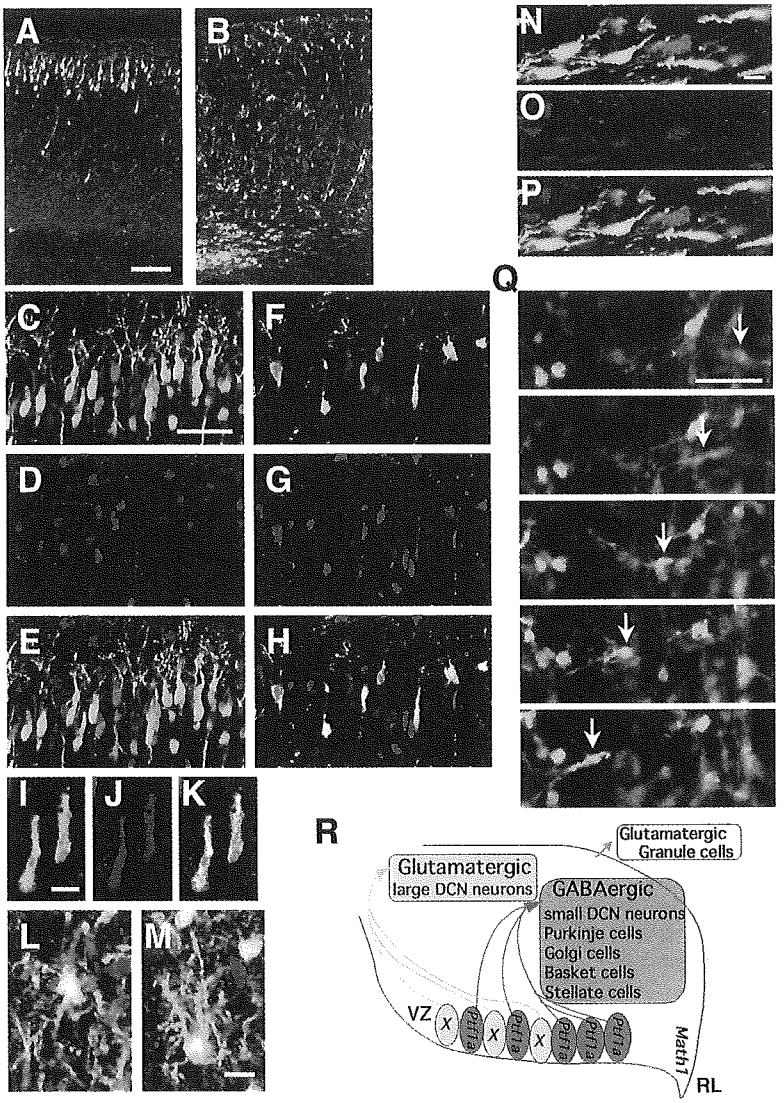

Figure 6. Introduction of *Ptf1a* into the Dorsal Telencephalon

GFP (green) and GABA (red) are labeled. (A–P) Sections of P0 wild-type mice electroporated with control (A and C–E) or *Ptf1a* (B and F–P). Higher-magnification view of the upper (C–H) and lower (I–K) cortical plate and the intermediate zone (N–P). (L and M) Representative GFP-enhanced images of *Ptf1a*-introduced cells in the cortical plate. (Q) Time-lapse panels of *Ptf1a*-introduced slice at intervals of 90 min. Arrows, tangentially migrating cell. Scale bars, (A and B) 100 μm, (C–H) 40 μm, (I–P) 10 μm, (Q) 50 μm. (R) A model for glutamatergic-GABAergic specification by bHLH proteins in the cerebellum. X, unknown bHLH protein. RL, Rhombic lip.

control cells in the upper side of the intermediate zone (Movie S2), the majority of *Ptf1a*-introduced cells either remained stationary or migrated tangentially (Figure 6Q and Movie S3). In addition, immunostaining revealed that *Ptf1a*-transfected cells did not express calbindin (see Figure S2H).

These findings suggest that *Ptf1a* introduction into neural precursors in the dorsal telencephalon can confer GABAergic characteristics on the progeny neurons, in terms of not only the neurotransmitter subtype, but also cell morphology and migratory behavior.

Discussion

Pathology of *cbll*

The primary defect observed in the *cbll* brain was specific inhibition of all types of GABAergic neuron production from the cerebellar VZ, whereas primary generation of granule cell precursors and neurons in the inferior olivary and pontine nuclei occurred. Granule cell precursors emerge from the rhombic lip and migrate along the dorsal surface of the cerebellar primordium, forming the EGL. However, in the mutant, they fail to differentiate into granule cells and gradually disappear, accompanied by apoptotic features. It has been suggested that Sonic Hedgehog (Shh) secreted from Purkinje cells is required for granule cell precursors to proliferate, differentiate, and survive in the cerebellum during development (Dahmane and Ruiz-i-Altaba, 1999; Lewis et al., 2004; Wallace, 1999; Wechsler-Reya and Scott, 1999). Primary inhibition of GABAergic neuron production may therefore account for the secondary gradual loss of the granule cell precursors and result in the lack of the entire cerebellar cortex in *cbll* adults.

The disappearance of the inferior olivary and pontine nuclei occurs abruptly and completely within a few days, postnatally, exhibiting apoptotic features in the *cbll* mutants. It is known that neurons in the inferior olivary and pontine nuclei extend their axons toward Purkinje cells (climbing fibers) and granule cells (mossy fibers), respectively. Because the survival of many types of neurons is known to be target dependent (Ben-